Dynamic temperature propagation in a pure fluid near its critical point observed under microgravity during the German Spacelab Mission D-2

J. Straub, L. Eicher, and A. Haupt
Institute A for Thermodynamics, Technical University Munich, Arcisstrasse 21, 80333 Munich, Germany
(Received 4 November 1994)

Diverging thermodynamic and transport properties of a near critical fluid have significant effects on heat and mass transport; the effects are still under investigation. These effects become visible especially in experiments carried out under microgravity conditions because in the absence of gravity, buoyancy induced convection is suppressed. According to the "critical slowing down" hypothesis, even longer thermal relaxation times are predicted for experiments under reduced gravity conditions than for that on earth. Early experiments under microgravity showed a fast dynamic temperature propagation. More recently, this effect has been called the "piston effect," or "critical speeding up." The final thermodynamic equilibration of temperature and density is still very slow according to a diffusion process of heat and mass. During the German Spacelab Mission D-2 in 1993, the calorimeter HPT-HYDRA, which was designed for measurements of the specific heat at constant volume c_V, was also used for investigations of the dynamic temperature propagation. The spherical cell filled with SF_6 at critical density was pulsewise heated, which caused a temperature increase in the fluid of about 10 mK. The temperature propagation in the fluid was monitored with a resolution of 10 μK at three different radial positions in the fluid and at the wall of the cell. The experiments were carried out at 39 different temperatures in the region of 0.03 K $< |T - T_C| <$ 5.25 K. Approaching the critical temperature T_C, the temperature difference between the wall and the fluid decreases to zero in both the one phase and two phase regions. The experimental results in both the one phase region and two phase regions are in remarkably good agreement with numerical simulations and confirm the fast temperature propagation, which is predicted by the "piston effect" model quantitatively. In addition the phase separation process during cooling is explained with this model.

PACS number(s): 66.10.Cb, 65.70.+y, 44.30.+v, 05.70.Fh

I. INTRODUCTION

Usually, experiments in near critical pure fluids suffer under long thermal relaxation times. This effect is known as "critical slowing down." The comparatively fast temperature equilibration observed on earth (1g) was generally explained with the stirring effect of gravity induced buoyancy convection. In an experiment performed in 1984 under microgravity with the ballistic rocket TEXUS [1], where convection was excluded, the temperature propagation was still very fast. However, the density change close to the critical point was observed to be very slow [2]. Onuki and co-workers [3,4] explained the observed fast temperature propagation in the bulk fluid with an adiabatic, or, more correctly speaking, isentropic temperature propagation. For the homogeneous supercritical fluid, they developed a one dimensional analytical model, that describes the fast temperature response in the bulk fluid after a temperature step at the wall. With the assumption that the pressure propagates with the sound velocity, Boukari *et al.* presented a numerical solution [5] and after than an experimental test on Earth [6]. Zappoli *et al.* [7] included the pressure propagation in the fluid by solving the complete set of hydrodynamic equations and called the effect the "piston effect."

In a simple way this effect can be explained as follows. By heating or cooling the wall of a sample cell filled with a highly compressible, near critical fluid, the temperature in a thin boundary layer changes according to thermal diffusion. Due to its high expansion coefficient, the fluid in the boundary layer changes its volume and compresses (decompresses) the bulk fluid. This happens adiabatically without dissipation (and therefore isentropically) and causes an undelayed temperature change in the bulk. After that there is only a small temperature gradient at the wall and no gradient in the bulk. This process is completely different than that of heat transfer by conduction. Recent experiments [8,9,17] have confirmed these considerations qualitatively.

In this paper we present an experiment carried out during the Second German Spacelab Mission *D*-2 in 1993 with the HPT-HYDRA calorimeter, which confirms the fast dynamic temperature propagation quantitatively. A spherical cell filled with pure SF_6 at critical density was heated pulsewise and the temperature propagation in the fluid was observed at three radial positions. Numerical simulations using the experimental boundary conditions are in very good agreement with the experiments.

II. THEORETICAL APPROACH

The Fourier equation generally used for the description of diffusive heat conduction is valid only for incompressible substances or for a system kept at constant pressure. A critical fluid, however, is highly compressible, and therefore the complete hydrodynamic equations have to

be considered. Zappoli *et al.* [7] presented a complete solution. To describe the fluid properties he used the van der Waals equation, because solving the complete set of hydrodynamic equations with an equation of state for a real fluid requires extremely long computation time.

Boukari *et al.* [5] reduced the momentum equation to the assumption that the pressure in the system is constant over the whole sample volume and therefore only time dependent. This is allowed because the sound velocity is still high close to the critical point (e.g., 50 $m\,s^{-1}$ at $T-T_C=0.01$ K). Neglecting the velocities in the fluid, the conservation of energy is described by the change of the local entropy s:

$$\rho T\frac{\partial s}{\partial t}=\nabla\lambda\cdot(\nabla T)\ , \tag{1}$$

with λ the thermal conductivity, t the time, ρ the density, and T the temperature. Assuming local equilibrium, the change of entropy s is expressed by

$$\frac{\partial s}{\partial t}=\left[\frac{\partial s}{\partial T}\right]_p\frac{\partial T}{\partial t}+\left[\frac{\partial s}{\partial p}\right]_T\frac{\partial p}{\partial t}\ , \tag{2}$$

with p the pressure. Using the Maxwell relation

$$\left[\frac{\partial s}{\partial p}\right]_T=\frac{1}{\rho^2}\left[\frac{\partial \rho}{\partial T}\right]_p\ , \tag{3}$$

the definition of the specific isobaric heat capacity

$$c_p=T\left[\frac{\partial s}{\partial T}\right]_p\ , \tag{4}$$

and the thermodynamic relation

$$c_p-c_V=-\frac{T}{\rho^2}\left[\frac{\partial p}{\partial T}\right]_\rho\left[\frac{\partial \rho}{\partial T}\right]_p\ , \tag{5}$$

Eq. (1) can be transformed into

$$\frac{\partial T}{\partial t}=\frac{1}{\rho c_P}\nabla(\lambda\cdot\nabla T)+\left[1-\frac{c_V}{c_P}\right]\left[\frac{\partial T}{\partial p}\right]_\rho\frac{\partial p}{\partial t}\ . \tag{6}$$

Approaching T_C the diverging isobaric heat capacity c_p obviously diminishes the influence of the first term on the right-hand side of Eq. (6), which describes the thermal diffusion. The influence of the second term increases and causes an isentropic temperature change in the bulk fluid. For an incompressible fluid $c_V/c_p=1$, the pressure term equals zero and Eq. (6) corresponds to the Fourier equation

To determine the pressure change we write

$$\frac{\partial \rho}{\partial t}=\left[\frac{\partial \rho}{\partial T}\right]_p\frac{\partial T}{\partial t}+\left[\frac{\partial \rho}{\partial p}\right]_T\frac{\partial p}{\partial t}\ . \tag{7}$$

Due to mass conservation the integral of the density change over the sample volume must be equal to zero. As the pressure is assumed to be only time dependent, Eq. (7) can be transformed to

$$\frac{\partial p}{\partial t}=\frac{\int_V\rho\alpha_P(\partial T/\partial t)dV}{\int_V\rho\chi_T dV}\ , \tag{8}$$

with α_p as the isobaric expansion coefficient and χ_T as the isothermal compressibility.

Equations (6) and (8) can only be solved numerically. Within that limitation, experimental conditions with time dependent boundary conditions can be approximated numerically. Therefore we have used this approach for the simulation of our experimental results.

Because of the rotational symmetry of our spherical sample cell with radius R (Fig. 1), we treated the problem in one dimension with the spatial coordinate x, which is counted in the radial direction with $x=0$ at the sample wall and $x=R$ in the center of the cell. Considering the spherical shape of the sample cell, Eq. (6) changes to

$$\frac{\partial T}{\partial t}=\frac{1}{(R-x)^2}\frac{\partial}{\partial x}\left[\lambda(R-x)^2\frac{\partial T}{\partial x}\right]+\left[1-\frac{c_V}{c_p}\right]\left[\frac{\partial T}{\partial p}\right]_\rho\frac{\partial p}{\partial t} \tag{9}$$

and Eq. (8) to

$$\frac{\partial p}{\partial t}=\frac{\int_{x=0}^{R}\rho\alpha_p\frac{\partial T}{\partial t}(R-x)^2dx}{\int_{x=0}^{R}\rho\chi_T(R-x)^2dx}\ . \tag{10}$$

Equations (9) and (10) are solved iteratively for the two variables time t and space x. As the time variable boundary condition we used the measured temperature rise of the cell wall. For completeness, the analytical solution of Onuki *et al.* [3] is presented in a complete and transformed description. It describes the temperature response in the fluid caused by a temperature step from the initial temperature T_0 to the final temperature T_W at the wall:

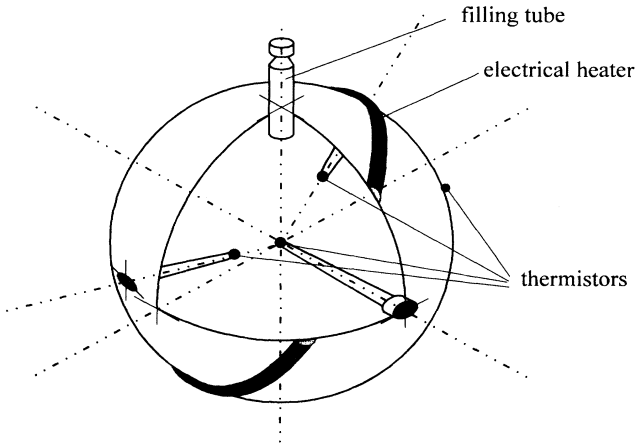

FIG. 1. Sketch of the sample cell, a hollow sphere of 20 mm diameter with a wall thickness of 0.4 mm, made of copper with a gold layer inside and outside, one thermistor at the outer surface of the wall, and three thermistors in the fluid at different radial positions.

$$\frac{T_W - T(x,t)}{T_W - T_0} = \exp\left[-\left[\frac{c_P}{c_V} - 1\right]\sqrt{D_{\text{th}}}\frac{A}{V}\left[\frac{4}{\pi}\right]^{1/2} t^{1/2}\right] \times \operatorname{erfc}\left[\frac{x}{2\sqrt{D_{\text{th}} t}}\right]. \quad (11)$$

Here A is the heating area of the sample, V is the total volume, $T(x,t)$ is the actual temperature in the fluid, and D_{th} is the thermal diffusivity. Here the spatial coordinate x is perpendicular to the heating area A. The exponential function describes the temperature change in the bulk. The erfc in Eq. (11) describes the temperature profile of the boundary layer at the wall. It is the analytic solution of the Fourier equation for heat conduction into a half-infinite body. It is valid as long as the boundary layer is not extended to the center of the sample cell ($x < R$). For $x/(2\sqrt{D_{\text{th}} t}) > 2$ the erfc tends to unity, and Eq. (11) describes the isentropic temperature change in the bulk fluid. It must be emphasized that Eq. (9) is only valid for an ideal temperature step that cannot be realized in experiments and therefore discrepancies occur when comparing the predictions with experimental results.

However, from this approach one can estimate the influence of the fluid properties and the geometry of the sample cell on the equilibration process. With an increasing ratio of the heating area to the total sample volume, A/V, the temperature change of the bulk is accelerated. This fact should be considered in the design of experiments to obtain a measurable temperature response in the bulk by a small temperature change at the heated wall. As $(c_p/c_V)\sqrt{D_{\text{th}}} \sim \tau^{-0.68}$ diverges along the critical isochore for $\tau = |(T - T_c)/T_c| \to 0$, the temperature propagation becomes faster as it approaches the critical point.

III. EXPERIMENTAL SETUP

During 40 hours of altogether 220 hours experimental time of the D-2 Mission we used the HPT-HYDRA calorimeter setup described in [10] to also perform experiments on temperature propagation. The spherical cell (see Fig. 1; inner radius $R = 9.6$ mm; wall thickness: 0.4 mm; wall material: copper) filled with pure SF_6 (critical temperature of SF_6: $T_C = 318.733$ K) at critical density was mounted in the center of a three stage thermostat. To avoid uncontrolled heat loss to the surrounding stage, vacuum of high quality was maintained and the temperature difference between the sample cell and the surrounding shell until the beginning of the heat pulse was set to zero.

At 39 different temperatures in the range $0.03 \text{ K} < |T - T_C| < 5.25$ K the cell was heated for 10 s with a power of 3.85 mW and the temperature response was measured with four thermistors (diameter: 0.35 mm; time constant: 0.1 s) with a measuring frequency of 1.66 Hz. One thermistor was fixed at the outer surface of the spherical cell, and three were in the fluid at different distances from the wall (3.2, 6.0, and 8.4 mm). Each heat pulse caused a temperature increase of cell and fluid between 8 and 15 mK, depending on the distance from T_C.

This heater was realized by a wound wire, which was pasted on the outer surface of the cell along a great circle. The thermal conductivity of the adhesive is given by 1.0 $\text{W m}^{-1}\text{K}^{-1}$. The maximum temperature difference in the cell wall, which occurred at the end of the heat pulse, was calculated to be less than 1 mK. The thermistor for measuring the wall temperature was mounted at a distance of about 5 mm from the heater, where the temperature equaled the mean temperature of the wall to within 0.1 mK. So the whole wall of the cell can be treated as an almost isothermal heating area and thus we obtained a large ratio $A/V = 3/R$.

There was only one amplifier installed for the temperature measurement of the four thermistors. Since its transition time constant was 3.9 s, it was not possible to switch between them during one heat pulse without loss of information. Therefore we performed four identical heat pulses at each temperature level and measured only one thermistor at each pulse.

IV. EXPERIMENTAL RESULTS

A. One phase region above T_C

In Figs. 2(a) and 3(a) the temperature response during and after the 10 s heat pulse is shown at temperatures of $T - T_C = 4.75$ and 0.1 K, respectively. The solid line represents the temperature T_W at the wall of the cell, and the symbols the resulting temperature in the fluid at the various positions as indicated. The dashed line shows the result of the numerical calculation according to Eqs. (9) and (10) with $T_W(t)$ as the boundary condition at $x = 0$. Note that at $T - T_C = 4.75$ K (Fig. 2) the three temperatures in the fluid at the positions $x = 3.2$, 6.0, and 8.4 mm are almost equal, while between the wall and the bulk a reasonable temperature difference is developed in a thin boundary layer; see Fig. 2(b). Here the calculated temperature distribution in radial direction after the 10 s heat pulse is plotted. The thickness of the thermal boundary layer established by diffusion is less than 0.5 mm. The uniform temperature increase in the bulk is caused by the isentropic compression as a consequence of the expanding boundary layer. Because of the thermal resistance of the adhesive, the measured temperature response is delayed by about 2 s and at the end of the pulse the temperature increase continues for the same amount of time. As we could not measure the thickness of the adhesive layer between the heater and the cell wall reliably, we determined the transient behavior between heater and cell by a reference experiment with an empty cell. It must be pointed out that this time delay has no influence on our result, because in the numerical calculation the actual recorded wall temperature itself is used as a boundary condition. It is demonstrated that the calculated curve follows exactly the measured values. This confirms the hypothesis of the isentropic temperature propagation and the physical correctness of the numerical modeling.

At $T - T_C = 0.1$ K (Fig. 3) nearly no temperature difference between the wall and the bulk fluid is observed. The calculated temperature course follows exactly the measured courses. After 10 s the calculated temperature difference between wall and bulk is about 0.2 mK and the

thickness of the boundary layer is 0.2 mm; see Fig. 3(b). That means that because of the diverging thermal conductivity λ, the thermal resistance between wall and fluid is nearly zero, although the thermal diffusivity is very low. At $T-T_C=0.1$ K the thermal conductivity λ of the fluid is 0.4 $\mathrm{W\,m^{-1}K^{-1}}$ and its thermal diffusivity $D_{\mathrm{th}}=3.6\times10^{-10}\,\mathrm{m^2\,s^{-1}}$, compared to $\lambda=0.08$ $\mathrm{W\,m^{-1}K^{-1}}$ and $D_{\mathrm{th}}=6.5\times10^{-10}$ $\mathrm{m^2\,s^{-1}}$ at $T-T_C=4.75$ K. Closer to the critical point this temperature difference becomes so small that within the uncertainty of the measurement no temperature differences were observed. Therefore no experiments closer to T_C are presented here.

B. Two phase region below T_C

Below the critical point the phase distribution under microgravity is not as obvious as under 1g conditions. From several experiments, we know that the liquid phase wets the wall and the vapor forms a bubble in the liquid. Therefore in a spherical cell filled with a fluid at critical density one will expect a phase distribution where the vapor bubble, which is not necessarily centered, takes almost half of the cell volume and is surrounded by a liquid layer at the wall. In our cell the phase distribution is disturbed by the thermistors, but we do not know in what way. However, for the following consideration and for the numerical simulations we assume a symmetric phase distribution with the bubble in the center of the cell surrounded by a liquid layer of about 2 mm thickness.

In the two phase region a heat pulse causes different temperature responses in the liquid (vapor). We can assume that the pressure rise caused by the expansion of the thermal boundary layer is equal in both phases, but even close to T_C the thermophysical properties are different in both phases. In our special case the isentropic temperature pressure coefficient $(\partial T/\partial p)_s$ of the vapor is larger than that of the liquid. Therefore, for the same pressure increase, the isentropic temperature increase in the vapor is higher than in the liquid.

The T-s phase diagram (Fig. 4) explains this effect: Starting from the saturation state of both phases (1) a thin liquid boundary layer is heated up, penetrates with increasing entropy into the metastable region, and ex-

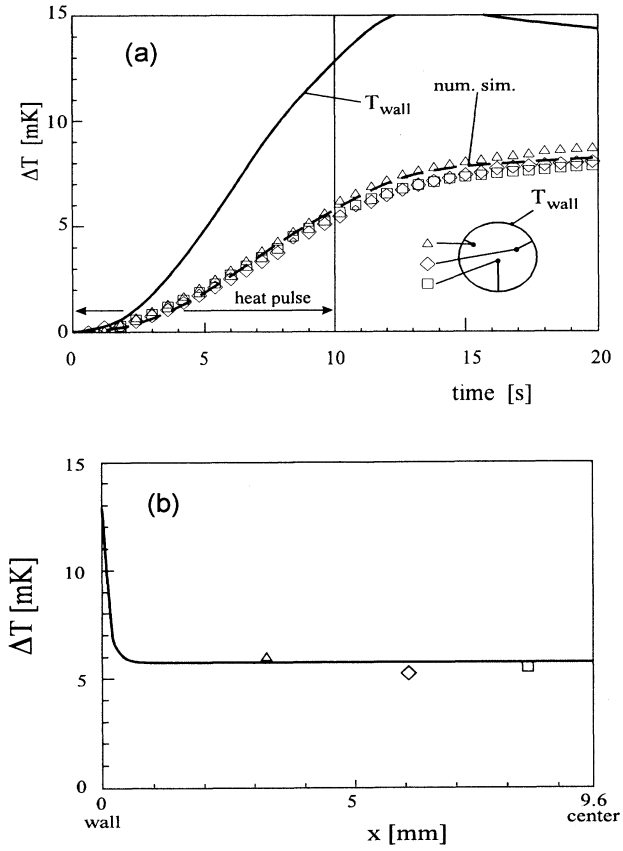

FIG. 2. (a) Temperature response in the fluid (triangles, squares, diamonds) and at the sample wall (solid line) during and after the heat pulse at $T-T_C=4.75$ K compared to the numerical simulation for the bulk fluid (dashed line). (b) Calculated temperature distribution (solid line) at the end of the heat pulse after 10 s. The measured temperatures at this time are marked with the corresponding symbols.

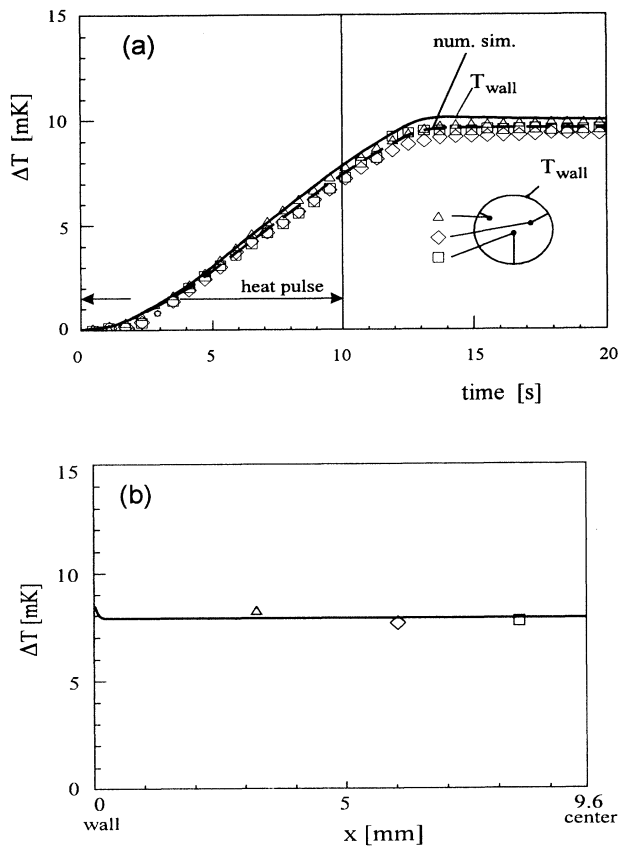

FIG. 3. (a) Temperature response in the fluid (triangles, squares, diamonds) and at the sample wall (solid line) during and after the heat pulse at $T-T_C=0.1$ K compared to the numerical simulation (dashed line). (b) Calculated temperature distribution (solid line) at the end of the heat pulse after 10 s. The measured temperatures at this time are marked with the corresponding symbols.

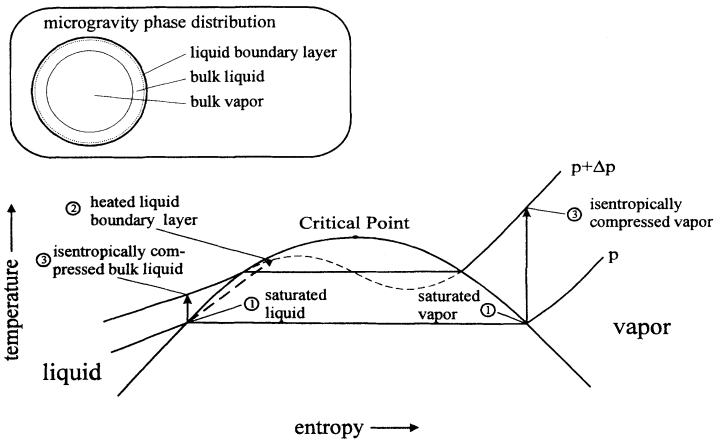

FIG. 4. The process of heating below the critical point, schematically explained in a *T-s* phase diagram. Both bulk phases are compressed isentropically.

pands to (2). With that the saturated bulk fluid (1)—both liquid and vapor—is compressed isentropically and heated up to (3). Due to the asymmetry of the isobars in the *T-s* phase diagram the temperature increase of the vapor is larger than that of the liquid. The vapor is superheated and the liquid subcooled now; phase transition with mass transport occurs only at the interface. It must be emphasized that by heating up a two phase system both phases are driven away from equilibrium and therefore long thermal relaxation times are required, as was observed on earth and in space [1,2].

In the numerical calculation we assume that the temperature at the interface is always at saturation according to the calculated pressure of the system. This assumption can be justified, because a small deviation from the equilibrium yields strong evaporation or condensation in such a way that the equality of the chemical potential at the interface follows immediately. The bulk liquid and vapor follow the equilibration by a slow process of heat and mass diffusion. This assumption is consistent with experimental observations of Straub [11]. He observed that in a two phase system the densities at the interface of both liquid and vapor follow immediately a temperature rise and equal the corresponding saturation densities. For the short time of our calculation, however, the mass transport across the interface can be neglected. From the calculation we receive the temperature response separately in both phases and at the interface; see Fig. 5. A model and numerical simulations, where the mass transport across the interface is considered, is presented in [12].

The measured temperature response of the thermistors at $x = 3.2$ and 8.4 mm follow the predicted course of the saturation temperature; that of the thermistor at $x = 6.4$ mm is close to the predicted one of the vapor. From this observation we conclude that the bubble is not centered in the sphere, but must be dislocated by the thermistors itself.

This dislocation of the bubble is observed in all experiments for $T - T_C < -2$ K. At about $T - T_C = -1$ K and closer to T_C the measured temperature courses of all three thermistors are equal. Within the uncertainty of the measurement they lie between the predicted temperature of the liquid and the saturation temperature (Fig. 7). This leads to the assumption that close to T_C the thermistors are wetted with liquid caused by the perfect wetting near the critical point as described in [13].

After the D-2 mission we performed the experiments with the same setup under Earth conditions. Here the phase distribution is obvious and we know which thermistor is immersed in the liquid (vapor). Figure 6

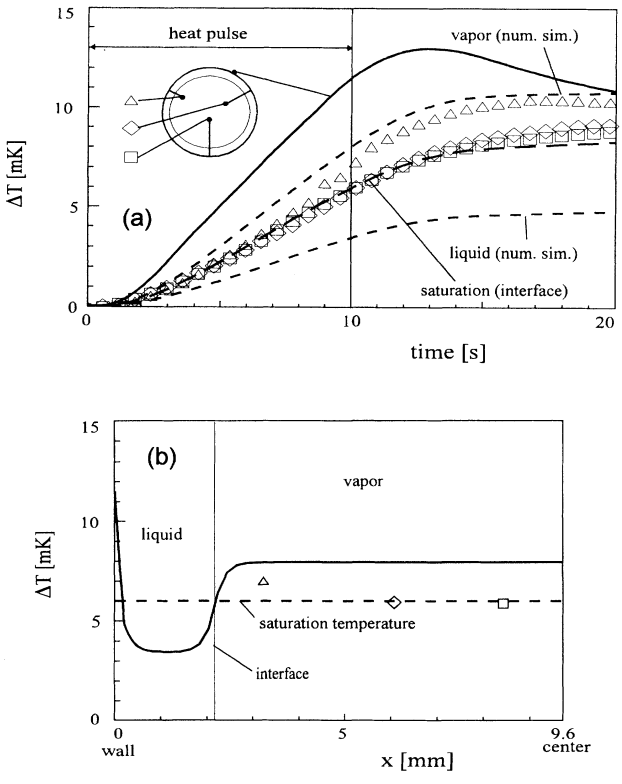

FIG. 5. (a) Temperature response in the fluid (triangles, squares, diamonds) and at the sample wall (solid line) during and after the heat pulse at $T - T_C = -2.25$ K compared to the calculated temperature courses of liquid and vapor and at the interface (dashed lines). (b) Calculated temperature distribution (solid line) at the end of the heat pulse after 10 s in both phases. The measured temperatures at this time are marked with the corresponding symbols.

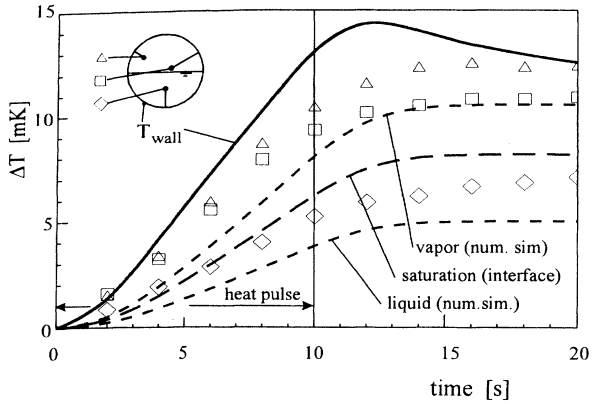

FIG. 6. Experimental run under Earth conditions at $T-T_C=-2.25$ K. The temperature response in the fluid (triangles, squares, diamonds) and at the sample wall (solid line) during and after the heat pulse is compared to the calculated temperature courses of liquid and vapor and at the interface (dashed lines).

shows the measured temperature response at $T-T_C=-2.25$ K compared to our numerical simulations.

For both phases the measured temperature response is faster than that predicted by our simulations. This is explained by the influence of buoyancy convection, which accelerates the temperature propagation. But it is remarkable that the temperature difference between the two phases in the experiment is equal to the calculated one. This observation was made in all experimental runs below T_C; see Fig. 7.

C. Discussion of the experimental results

All results of the experiments at microgravity and 1g are shown in Fig. 7 for the temperature range of the experiment. For comparison we define a dimensionless temperature difference $(T_{\text{wall}}-T_{\text{fluid}})/(T_{\text{wall}}-T_{\text{initial}})$ at the end of the 10 s heat pulse. Above T_C the numerical simulation is in very good agreement with the experimental results obtained under reduced gravity. Even under Earth conditions the agreement is good up to $T-T_C=0.5$ K. It must be emphasized that in the numerical simulation no convection effects are considered. For $T-T_C>0.5$ K we observed on Earth a slightly faster temperature propagation than predicted. We explain this with the beginning influence of convection. But even here the isentropic temperature propagation is the dominant transport process.

Below T_C the microgravity results up to $T-T_C=-2.0$ K are more or less between the calculated temperature responses for vapor and saturation. Mostly, two of the thermistors are close to the behavior of the saturation temperature. That means that they are located very close to the interface. One thermistor seems to be more immersed into the vapor phase. We tentatively suspect that the thermistors squeeze the vapor bubble into one side of the spherical cell. Between $T-T_C=-1.0$ K and $T=T_C$ there is no significant temperature difference between the thermistors and they show all the predicted behavior of the liquid. We explain this with the perfect wetting near the critical point [13]. So all thermistors are wetted by liquid and as a consequence they see the temperature of the liquid. In the 1g experiments we know the position of the thermistors; see Fig. 7. Between $T-T_C=-1$ K and $T-T_C=0$ K the measured temperature response follows very well the predictions of our simulation. At lower temperatures the influence of convection becomes visible and the temperature propagation is accelerated in the vapor phase more than in the liquid. As we observed by heating a transparent sample cell, separate convection rolls divided by the interface will develop in liquid and vapor and no mass flow will cross the interface. As discussed above, the isentropic piston effect dominates the temperature propagation for temperatures $|T-T_C|<1$ K. In this region convection plays a minor roll, because the boundary layer created by diffusion is very thin and does not lead to a significant stirring effect within the short time of the experiment.

V. COOLING AND PHASE SEPARATION

In the preceding section we have discussed only the results of heating. In the one phase region, as long as no density stratification is established and cooling does not go below T_C, the temperature propagation can be calculated with Eqs. (7) and (8).

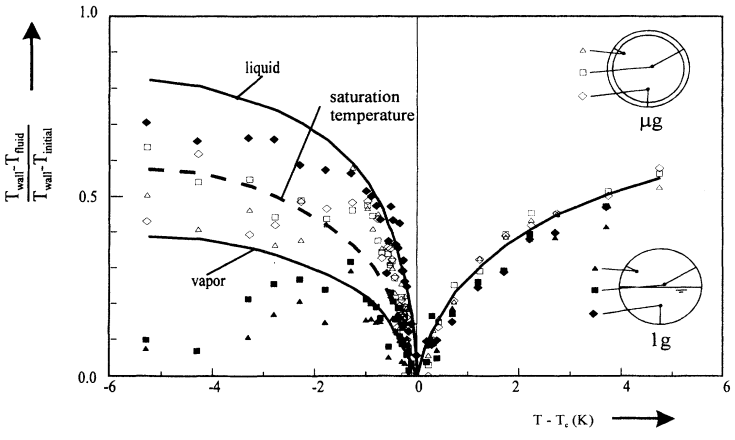

FIG. 7. Dimensionless temperature difference between wall and fluid after the heat pulse for all microgravity experiments (open symbols) and 1g experiments (filled symbols).

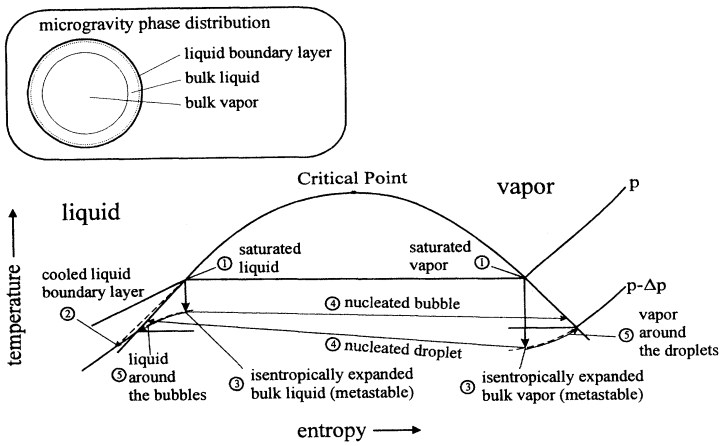

FIG. 8. The process of cooling and phase separation below the critical point, schematically explained in a (T-s) phase diagram.

In the two phase region during heating the vapor is superheated and the liquid subcooled and reasonable temperature differences occur between the two phases; see Fig. 4.

Cooling a two phase system is completely different. We demonstrate this in the T-s phase diagram (Fig. 8). From the two phase equilibrium state (1) the liquid boundary layer is cooled to (2) and its volume shrinks by the increase of density. The bulk fluid, both liquid and vapor, expands isentropically from (1) to (3) and penetrates into the metastable region. Only the interface will be nearly at equilibrium, which is determined by the total pressure of the system. In both phases homogeneous nucleation occurs and so simultaneously bubbles are formed in the liquid and droplets in the vapor (4). Due to the latent heat consumed (released) by the subsequent growth of these bubbles and droplets, the surrounding fluid comes back to the saturation condition (5). Bubbles and droplets coalesce and by continuing the cooling new bubbles and droplets are nucleated. By this process a large interface is formed in the bulk, which allows a fast exchange of heat and mass between both phases. Therefore a continuously cooled two phase system is always close to its equilibrium state, as opposed to a heated two phase system, which is driven away from equilibrium. This explains the hysteresis effects, which we observed during the measurement of the isochoric specific heat capacity under microgravity during the D-1 Mission [2] and the D-2 Mission [10] and under Earth conditions [14,15].

The continuous formation of bubbles and droplets can be observed on Earth by continuously cooling a visual cell filled with a pure fluid of critical density. Continuous boiling with rising of small bubbles in the liquid and simultaneous condensation with falling droplets in the vapor occurs. The same, without sedimentation, however, was observed in our early TEXUS experiment [1], in the Critical Point Facility (CPF) during the IML-1 Mission, during the USMP-2 Mission [16], and recently during the IML-2 Mission.

VI. CONCLUDING REMARKS

Our experiments conducted during the D-2 Mission in 1993 evidently confirm the presence of the fast isentropic temperature propagation both in the one phase region and in the two phase region. The well designed and controlled experiment determines a boundary condition with which a numerical simulation can be performed. The good agreement between the simulation and the experimental results confirms the fast temperature propagation, theoretically predicted by the "piston model," quantitatively. It is pointed out that, besides the fluid properties, the ratio between the heated area and the total sample volume is important for the temperature response in the bulk. Comparing experiments at 1g with microgravity experiments shows that close to the critical point the isentropic temperature change is dominant and the influence of convection is noticeable for $|T-T_C|>1$ K.

The observed temperature difference between liquid and vapor phase below T_C can also be predicted with the simulation and is explained in the T-s phase diagram. It is important to note that during heating both bulk phases are driven away from equilibrium while during cooling both phases are penetrating into the metastable region and by continuous nucleation a suspension of bubbles in the liquid and droplets in the vapor is created, which is always very near the equilibrium state. The different behavior of a two phase system during heating (cooling) explains the hysteresis observed in c_V measurements.

ACKNOWLEDGMENTS

This research was supported by Deutsche Agentur für Raumfahrtangelegenheiten (DARA), Support No. QV8948. The authors want to thank the crew of the Space Shuttle Columbia STS 55, the responsible persons of the company Kayser-Threde, Munich, the operations control team of DLR and NASA, and all colleagues and students for their outstanding engagement for the HPT-HYDRA experiment during the D-2 Mission.

[1] K. Nitsche and J. Straub, in *Proceedings of the Sixth European Symposium on Material Sciences under Microgravity Conditions, Bordeaux, France, 1986* (European Space Agency, Paris, 1987). Vol. SP-256, p. 109.
[2] J. Straub and K. Nitsche, Fluid Phase Equil. **88**, 183 (1993).
[3] A. Onuki, H. Hao, and R. A. Ferrell, Phys. Rev. A **41**, 2256 (1990).
[4] A. Onuki and R. A. Ferell, Physica A **164**, 245 (1990).
[5] H. Boukari, J. N. Shaumeyer, M. E. Briggs, and R. W. Gammon, Phys. Rev. A **41**, 2260 (1990).
[6] H. Boukari, J. N. Shaumeyer, M. E. Briggs, and R. W. Gammon, Phys. Rev. Lett. **65**, 2654 (1990).
[7] B. Zappoli, D. Bailly, Y. Garrabos, B. LeNeindre, and D. Beysens, Phys. Rev. A **41**, 2264 (1990).
[8] H. Klein, G. Schmitz, and D. Woermann, Phys. Rev. A **43**, 4562 (1991).
[9] P. Guenoun, B. Khalil, D. Beysens, F. Kammoun, B. LeNeindre, Y. Garrabos, and B. Zappoli, Phys. Rev. E **47**, 1531 (1993).
[10] J. Straub and A. Haupt, Int. J. Thermophys. (to be published).
[11] J. Straub, Dissertation, Technische Universität München, Germany, 1965.
[12] J. Straub and L. Eicher, Phys. Rev. Lett. (to be published).
[13] M. R. Moldover and R. W. Gammon, J. Chem. Phys. **80**, 528 (1984).
[14] K. Nitsche, Dissertation, Technische Universität München, Germany, 1990.
[15] J. Straub, A. Haupt, and K. Nitsche, Fluid Phase Equil. **88**, 123 (1993).
[16] R. W. Gammon (private communication).
[17] M. Bonetti, F. Perrot, D. Beysens, and Y. Garrabos, Phys. Rev. E **49**, 4779 (1994).